International Journal of Coal Geology 138 (2015) 103–112

Contents lists available at ScienceDirect

International Journal of Coal Geology

journal homepage: www.elsevier.com/locate/ijcoalgeo

The effect of analytical particle size on gas adsorption porosimetry of shale

Yanyan Chen [a,b,*], Lin Wei [b], Maria Mastalerz [c], Arndt Schimmelmann [b]

[a] Research Institute of Petroleum Exploration & Development, PetroChina, Beijing 100083, China
[b] Department of Geological Sciences, Indiana University, Bloomington, IN 47405-1405, USA
[c] Indiana Geological Survey, Indiana University, Bloomington, IN 47405-2208, USA

ARTICLE INFO

Article history:
Received 6 June 2014
Received in revised form 23 December 2014
Accepted 23 December 2014
Available online 30 December 2014

Keywords:
Shale
Porosity
Adsorption
Kerogen transformation
Particle size

ABSTRACT

Gas storage capacity and gas producibility of shale gas reservoirs are critically limited by shale porosity. In spite of its importance, porosimetric characterization of shale remains challenging due to highly heterogeneous structures, small average pore sizes, and wide pore size distributions. This study utilizes low-pressure N_2 and CO_2 gas adsorption porosimetry to investigate the evolution of micro- and mesopores in a suite of 11 New Albany Shale samples across a wide range of thermal maturity corresponding to vitrinite reflection R_o values from 0.35 to 1.41%. Mesopore volumes follow a nonlinear evolutionary path starting with a maximum in immature shale (sample 472-1). Subsequent intermittent minima in mesopore volumes during early and late maturity are consistent with the transformation of kerogen during the early mature stage (sample 554-2) and secondary cracking of bitumen/oil at the late mature stage (sample IL2), respectively. Micropore volumes display a varying trend throughout thermal maturation, and are significantly controlled by total organic carbon contents. Both meso- and micropore volumes are positively correlated with clay content and tend to decrease with an increase in feldspar content.

A reduction in grain size of shale samples for gas adsorption porosimetry prominently enhances mesopore volumes, whereas the effects on micropore volumes are variable. These findings may be associated with the fact that smaller particles are able to attain complete adsorption equilibrium quickly, which in turn reduces experimental artefacts during gas adsorption porosimetry. Crushing of shale not only alters the shape of gas adsorption hysteresis loops, but also tends to tighten the openings of hysteresis loops by enhancing the connectivity of pores and reducing the likelihood of gas being trapped during desorption.

1. Introduction

Successful exploration and recovery of natural gas from low-permeability unconventional reservoirs such as shales require an understanding of rock porosity. In spite of this importance, accurate porosimetric characterization of shales remains challenging due to highly heterogeneous structures across macro- to microscales, small average pore sizes, and wide pore size distributions (Chalmers et al., 2012; Kuila and Prasad, 2013; Loucks et al., 2009; Mastalerz et al., 2012, 2013). The quantification of pores in shales by gas adsorption techniques is further complicated by limited pore connectivity and partial filling or blocking of pores with water or bitumen (Clarkson et al., 2012; Mastalerz et al., 2013).

Even bioturbated, seemingly homogeneous shales typically express heterogeneous distributions of organic and inorganic moieties with associated pores when viewed at a magnification that is commensurate with the small pores in fine-grained rocks (Schieber, 2010, 2011). Spatial variations in mineralogical composition and organic matter (OM) content across short distances in sediment cores are typically paralleled by variances in pore volumes and pore size distributions. For instance, carbonate-rich intervals of Gordondale Shale (Lower Jurassic, northeastern British Columbia, Canada) typically have lower total porosities than adjacent carbonate-poor and clay-rich mudrocks (Ross and Bustin, 2007). The presence of clays of the illite–smectite type is mainly responsible for micro- and mesopores in shales (Kuila and Prasad, 2013). Porous OM is an important contributor to total porosity in organic-rich shales and can host substantial micropore volumes that usually correlate positively with the total organic carbon (TOC) content (Chalmers et al., 2012; Loucks et al., 2009; Strąpoć et al., 2010). Mineral- and OM-associated pores show contrasting geometries and morphologies. For example, cross-sections of mineral-associated pores in Haynesville Shale are predominantly slit-like, whereas OM pores in the Barnett and Horn River shales are typically round or elliptical (Curtis et al., 2012).

Pores in OM have attracted growing interest as a significant component of pore systems in gas-bearing shales (Bernard et al., 2012; Curtis

* Corresponding author at: Department of Geological Sciences, Indiana University, Bloomington, IN 47405-1405, USA.
E-mail address: yanycheniu@gmail.com (Y. Chen).

http://dx.doi.org/10.1016/j.coal.2014.12.012
0166-5162/

et al., 2012; Loucks et al., 2009; Mastalerz et al., 2013). While some OM pores are a legacy of the cellular structure of precursor biological tissues (Loucks et al., 2012), much OM-associated pore space seems to relate to thermal transformations of kerogen, (pyro)bitumen, and liquid and gaseous hydrocarbons (Jarvie et al., 2007; Mastalerz et al., 2012, 2013; Ross and Bustin, 2009; Strąpoć et al., 2010). Understanding the evolution of OM porosity during thermal maturation is critical for predicting the ability of shales to produce and store fluid hydrocarbons (Curtis et al., 2012).

Pores are generally classified according to their diameters as micropores (<2 nm), mesopores (2–50 nm), and macropores (>50 nm; Sing et al., 1985). Based on their associations with mineral and organic particles, pores can also be classified as intergranular mineral pores, intragranular mineral and OM pores, and fracture pores (Loucks et al., 2012). Limitations of individual porosimetric methods to sections of the wide spectrum of pore sizes in shales make it necessary to use more than one porosimetric method in order to measure pore sizes from micropores to macropores (Sing et al., 1985). Various gas adsorption techniques using helium, nitrogen (N_2) and carbon dioxide (CO_2) are available to quantify surface areas and pore characteristics of shales (Lowell et al., 2004). Additional porosimetric approaches include small angle X-ray and neutron scattering (SAXS, SANS, and USANS; Cui et al., 2009; Mastalerz et al., 2012), mercury intrusion capillary pressure (MICP) porosimetry (Clarkson et al., 2013; Mastalerz et al., 2013), high resolution scanning and transmission electron microscopy (SEM, TEM; Chalmers et al., 2012; Loucks et al., 2012; Schieber, 2010), and Nuclear Magnetic Resonance (NMR; Borchardt et al., 2013). Although traditional SEM and TEM can theoretically image nanopores with diameters down to 1 nm, in practice such small pores cannot be adequately imaged electron-microscopically (Walters, 2013). Porosimetry of small pores from 0.35 nm to 300 nm typically relies on gas adsorption techniques for assessment of pore sizes, including the complete range of micro-, meso-, and macropores (Cui et al., 2009; Mastalerz et al., 2013).

Although gas adsorption porosimetry has been used broadly for the characterization of porosity in shales, mudrocks and other porous materials, surprisingly little is known about the influence of some fundamental parameters like the grain size of used rock material. Lab-based standardizations of grain size by individual research groups serve to generate reproducible data within each lab. Unfortunately, the use of different standard grain sizes calls into question direct comparisons of published data from different laboratories. A compilation of findings from recent gas adsorption-related studies (Table 1) documents conflicting conclusions from laboratories that used different particle sizes.

Following our previous investigation on porosity in New Albany Shale (NAS; Mastalerz et al., 2013), this study aims to (1) systematically explore the influence of particle size on porosimetric characterization of NAS via gas adsorption. Additional goals are to (2) improve the characterization on the evolution of NAS's porosity across a wider range of thermal maturity by including additional NAS samples with intermediate maturities, and (3) to characterize the influence of mineralogical and organic compositions on the NAS pore system.

2. Experimental section

This study utilizes 11 NAS samples across wide ranges of thermal maturity (R_o 0.35 to 1.41%) and TOC contents (2.37 to 21.5 wt.%) for porosimetric measurements, X-ray diffraction (XRD), organic petrography, and other analyses. Total porosity of the samples ranges from 1.0 to 9.1 vol.% (Table 2). NAS samples originate from coring locations shown in Fig. 1. Cores without signs of weathering or oxidation have been archived by the Indiana Geological Survey and the Illinois State Geological Survey.

2.1. Low-pressure gas adsorption measurements

Each of the 11 shale samples was carefully hand-crushed and sieved to generate three size fractions of 4, 20 and 60 mesh. The resulting 33 samples were subsequently analyzed via N_2 and CO_2 low-pressure gas adsorption on a Micromeritics ASAP-2020 apparatus to obtain information about mesopores and micropores, respectively. Shale samples were automatically degassed at ~110 °C in vacuo for about 14 h to remove adsorbed moisture and volatile matter. Degassed sample aliquots weighing 1–2 g were exposed to N_2 at the temperature of liquid nitrogen (−196 °C) or to CO_2 near 0 °C along a series of precisely controlled gas pressures. N_2 and CO_2 adsorption volumes were measured over the relative equilibrium adsorption pressure (P/P_o) range of 0.050–0.995, where P_o is the condensation pressure of N_2 or CO_2 at laboratory conditions, and P is the actual gas pressure.

N_2-based adsorption data collected on shale size fractions were interpreted using Brunauer–Emmett–Teller (BET) analysis for surface area and Barrett–Joyner–Halenda (BJH) analysis for pore size distributions (Mastalerz et al., 2013). CO_2-based adsorption data were interpreted using Dubinin–Astakhov (D–A), Dubinin–Radushkevich (D–R), and density functional theory (DFT) pore size distribution models (Gregg and Sing, 1982). These calculations can be generated automatically by the instrument's computer software.

2.2. Organic petrography and X-ray diffraction analysis

Vitrinite reflectance R_o (%) measurements (maximally 25 points) were performed with a Leica optical microscope and an MSP200 photometry system. Total organic carbon (TOC) concentrations were quantified using a Leco analyzer. Independent quantitative mineralogical analyses of pulverized shale samples (ground wet with a micronizer to a grain size 5 μm) were performed with a Bruker D8 Advance XRD in the Department of Geological Sciences at Indiana University. The XRD was equipped with a Sol-X solid-state detector and a Cu X-ray tube operated at 40 kV and 30 mA. Shale powders were scanned from

Table 1
Summary of recent porosimetry via low-pressure N_2 and CO_2 gas adsorption techniques.

Literature	Particle size	Sample information	Relationship with total organic carbon (TOC)
Mastalerz et al. (2013)	4 mesh (4.75 mm)	New Albany Shale, USA	No relationship between TOC content and pore volume
Strąpoć et al. (2010)	60 mesh (250 μm)	New Albany Shale, USA	D–A micropore volume and total gas content correlate positively with TOC content
Ross and Bustin (2009)	60 mesh (250 μm)	Western Canadian Sedimentary Basin, Canada	Significant correlation between micropore volume and TOC content for Devonian–Mississippian shale but not for Jurassic shale.
Chalmers et al. (2012)	60 mesh (250 μm)	Barnett, Woodford, Haynesville, Marcellus, and Doig shales	No correlation between TOC content and micropore volume
Chalmers and Bustin (2012)	60 mesh (250 μm)	Shaftesbury Formation in northeastern British Columbia, Canada	Positive correlation between TOC content and porosity
Tian et al. (2013)	60–80 mesh (250–178 μm)	Lower Silurian shales in the Chuangdong Thrust Fold Belt, southwestern China	Total porosity increases with increasing TOC and clay contents
Mastalerz et al. (2012)	60 mesh (250 μm)	Springfield coal and New Albany Shale	Mesopore and micropore volumes increase with increasing TOC content

Table 2
Total porosity (vol.%) and mineralogical compositions (wt.%) of shale samples.

Sample	R_o (%)	TOC (wt.%)	Total porosity	Quartz	Dolomite	Calcite	Ankerite	All carbonates	Illite /smectite	Kaolinite	Chlorite	All clays	Albite	Sanidine	All feldspars	Pyrite
472-1	0.35	2.37	9.1	14.5	15.5	22.0	9.4	**46.9**	21.9	0.4	1.7	**24.1**	2.1	8.2	**10.3**	1.8
634-1	0.5	21.54	2.3	22.9	0.0	0.6	0.0	**0.6**	38.3	1.4	0.4	**40.1**	11.0	2.1	**13.1**	1.7
MM4	0.55	13	4.1	33.8	0.3	0.7	0.0	**1.0**	32.9	1.9	0.4	**35.2**	4.2	11.4	**15.6**	1.5
554-2	0.61	6.53	1.0	26.3	1.0	0.7	6.9	**8.5**	42.4	0.7	0.0	**43.1**	10.0	3.5	**13.5**	2.0
NA2	0.65	5.3	5.1	37.5	1.4	0.9	2.8	**5.1**	26.5	2.5	0.5	**29.5**	6.3	12.9	**19.2**	3.4
IL6	0.7	6.01	n.d.	35.4	0.4	1.1	0.0	**1.5**	36.1	1.8	0.2	**38.1**	5.5	12.8	**18.3**	0.8
IL4	0.83	6.2	1.1	24.8	3.5	1.2	0.0	**4.7**	39.3	2.1	0.1	**41.6**	5.0	16.3	**21.3**	1.4
IL5	1.15	4.29	1.5	27.8	18.1	10.5	0.0	**28.5**	23.4	0.0	0.0	**23.5**	5.3	8.6	**13.9**	2.0
IL3	1.27	5.5	2.5	35.7	0.1	1.6	0.0	**1.7**	36.5	0.1	2.4	**39.0**	3.9	13.3	**17.2**	0.9
IL2	1.3	3.3	3.5	22.3	4.9	0.0	0.0	**4.9**	0.0	0.5	1.1	**1.5**	33.9	32.7	**66.6**	1.4
IL1	1.41	6.29	3.5	19.9	11.7	0.0	0.0	**11.7**	1.2	0.7	0.7	**2.7**	25.2	27.0	**52.2**	7.3

n.d. = not determined.
Bold numbers indicate total concentrations of all carbonates, clays and feldspars.

2° to 70° using a count time of 2 s per 0.02° step. Multicomponent quantifications were achieved by Rietveld refinements using TOPAS software (Bruker, version 4.0).

3. Experimental results

3.1. Mineralogy

At the lower end of the wide spectrum of maturity represented in this study, the immature shale sample 472-1 features abundant carbonates (calcite, dolomite, and ankerite) but is lean in quartz and feldspar (Table 2). The sequence of shales with increasing maturity from 634-1 to MM4, 554-2, NA2, IL6, IL4, and IL3 exhibits rather consistent mineralogical compositions with low carbonate (<10 wt.%), intermediate feldspar (10–20 wt.%), and high quartz and clay (20–40 wt.%) contents. The pattern is broken by sample IL5 containing similar contents of quartz, clays, and carbonate (~25 wt.%), and slightly lower feldspar content (14 wt.%). The most mature shales IL2 and IL1 distinctively differ mineralogically from lower-maturity shales by their remarkably high feldspar (>50 wt.%) and low clay contents (Table 2).

3.2. Pore volume and pore size distribution

Micro- and mesopore volumes detected by low-pressure CO_2 and N_2 adsorption porosimetry are summarized in Table 3 and Fig. 2. Different particle sizes of the same shales express contrasting D–A micropore and BJH mesopore volume characteristics. The following paragraphs describe porosity characteristics of 60-mesh shales in detail, which are the most commonly used in related research, followed by a comparison among particle sizes.

3.2.1. Pore characteristics of 60-mesh samples as a function of thermal maturity

The evolution of BJH mesopore volumes ($V_{meso\text{-}60}$) along increasing thermal maturity follows a nonlinear path with multiple intermittent minima (Fig. 3). The mesopore volume is largest in the least mature

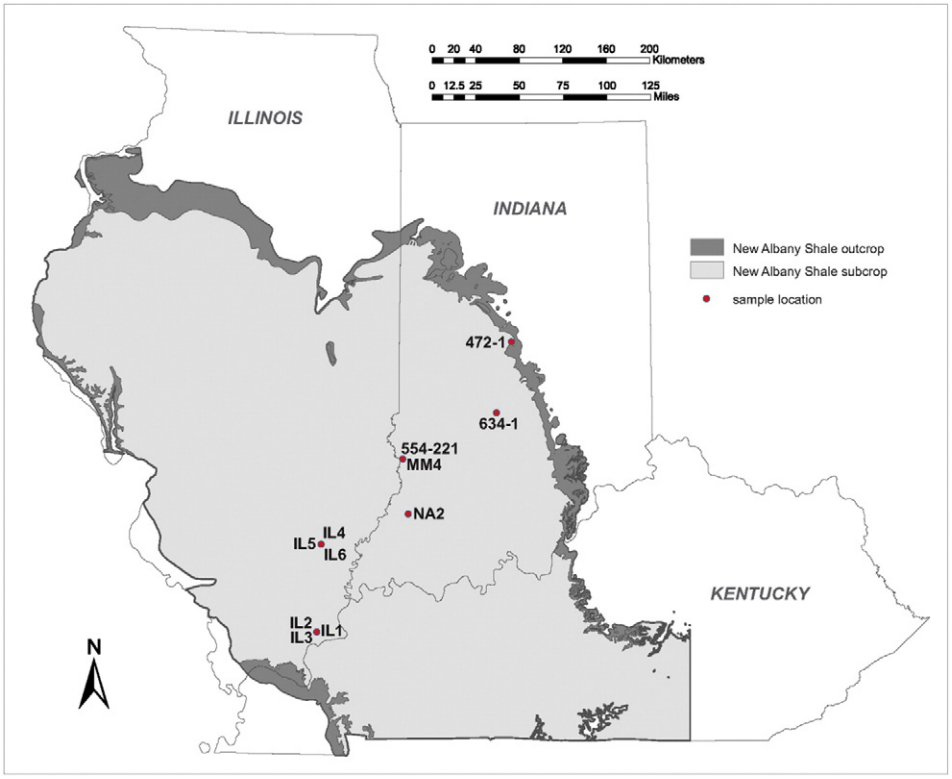

Fig. 1. Origin of New Albany Shale samples used in this study.

Table 3
Micropore and mesopore volumes of particle size fractions of shale samples.

Sample	60 mesh		20 mesh		4 mesh	
	D–A micropore volume (cm^3/g) ($V_{micro-60}$)	BJH mesopore volume (cm^3/g) ($V_{meso-60}$)	D–A micropore volume (cm^3/g) ($V_{micro-20}$)	BJH mesopore volume (cm^3/g) ($V_{meso-20}$)	D–A micropore volume (cm^3/g) ($V_{micro-4}$)	BJH mesopore volume (cm^3/g) (V_{meso-4})
472-1	0.0103	0.0265	0.0108	0.0222	0.0085	0.0208
634-1	0.0183	0.0177	0.0177	0.0097	0.0086	0.0032
MM4	0.0125	0.0153	0.0075	0.0030	0.0167	0.0080
554-2	0.0080	0.0112	0.0080	0.0033	0.0129	0.0002
NA2	0.0092	0.0149	0.0049	0.0043	0.0138	0.0052
IL6	0.0109	0.0137	0.0060	0.0041	0.0174	0.0005
IL4	0.0074	0.0141	0.0052	0.0033	0.0159	0.0002
IL5	0.0086	0.0130	0.0052	0.0023	0.0055	0.0004
IL3	0.0076	0.0140	0.0060	0.0051	0.0045	0.0026
IL2	0.0033	0.0055	0.0040	0.0037	0.0047	0.0019
IL1	0.0078	0.0095	0.0068	0.0044	0.0062	0.0036

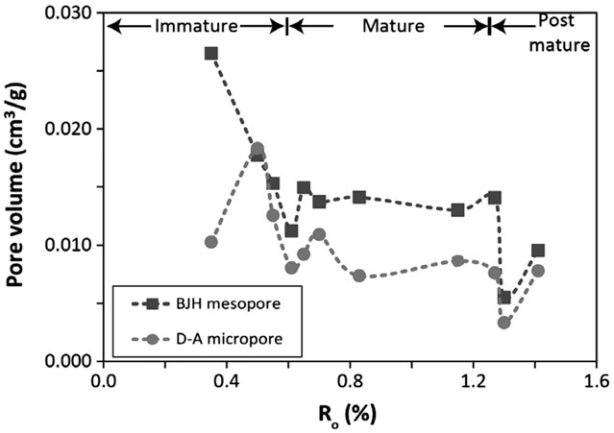

Fig. 3. Relationships between 60-mesh meso- and micropore volumes ($V_{meso-60}$ and $V_{micro-60}$) and vitrinite reflectance (R_o, %). The R_o ranges of different thermal maturation stages refer to Peters and Cassa (1994) and Mastalerz et al. (2013). Dashed lines were drawn to guide the eye.

sample 472-1, decreases intermittently with increasing thermal maturity and reaches the first minimum value in shale 554-2 (R_o 0.61%). Further maturation within the oil window witnesses an intermittent increase in mesopore volume, followed by a strong decrease to the absolute minimum in shale IL2 (R_o 1.3%). A final reversal raises N_2 adsorption in the most mature sample IL1. The N_2 adsorption isotherms are of type IV and exhibit hysteresis between relative pressures 0.420 and 0.995 in all 60-mesh shales (Fig. 4A). BJH mesopore size distributions are similar for all measured 60-mesh shale samples and are dominated by the pore size range of about 20–100 nm (Fig. 4B).

Micropore volumes ($V_{micro-60}$) express a varying trend with maturation (Fig. 3, Table 3). The most organic-rich shale 634-1 shows the strongest CO_2 adsorption as a proxy for largest $V_{micro-60}$ (Fig. 5A) and the largest DFT cumulative CO_2 adsorption volume (Fig. 5B). The patterns of DFT micropore size distribution across the pore size range from 0.4 to 1.1 nm are similar for all shales, with a distinct volumetric pore-width maximum at 0.82 nm (Fig. 6).

With increasing maturity, BET surface areas of 60-mesh samples determined by N_2 and CO_2 adsorption follow the nonlinear responses of $V_{meso-60}$ and $V_{micro-60}$, respectively (Table 4). The largest CO_2 BET equivalent surface area is apparent in the most organic-rich shale 634-1, whereas minima are observed in late mature IL4 and post mature IL2 (Table 4). CO_2 BET surface areas are mostly 0.2–2.3 times higher than those measured by N_2 adsorption, highlighting the strong contribution of micropores to surface areas in NAS samples. The average mesopore sizes in 60-mesh shales display a convex trend over increasing thermal maturity and possibly over increasing TOC content, while the average micropore sizes express respective concave profiles (Fig. 7).

3.2.2. Pore characteristics of 60-mesh samples as a function of mineralogy

Both micro- and mesopore volumes tend to be enhanced with increasing clay and decreasing feldspar contents (Fig. 8A, D), and show

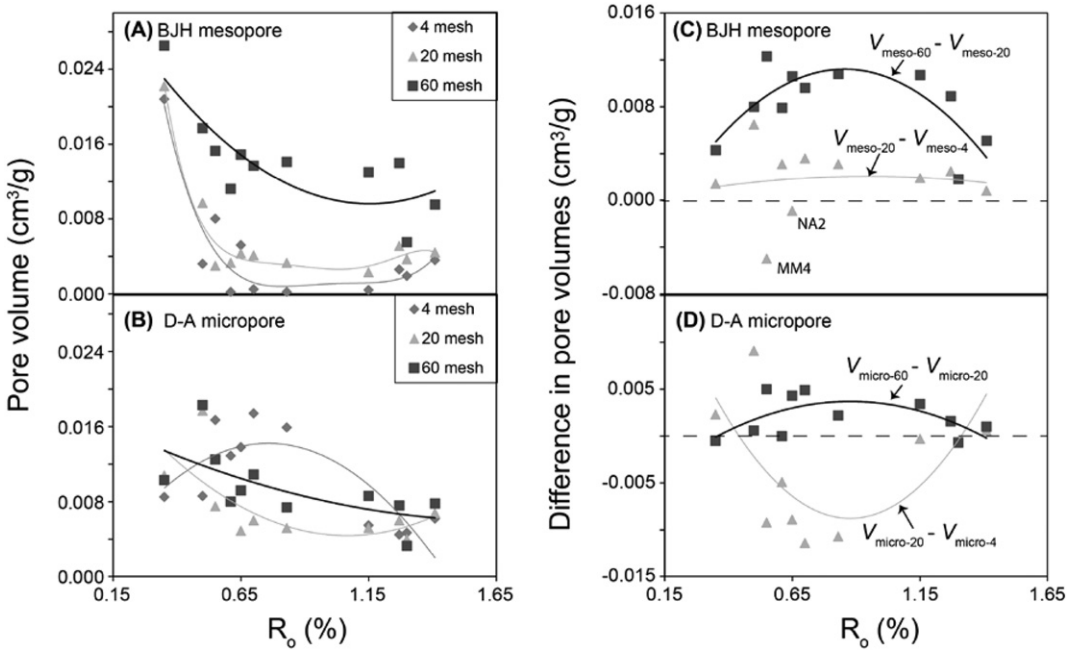

Fig. 2. Mesopore volumes (A) and micropore volumes (B) from varying particle size fractions plotted over vitrinite reflectance (R_0) as well as the relationships between differences in pore volumes and R_0 (C and D). Trend lines were drawn to guide the eye. Dashed lines in panels C and D indicate zero difference.

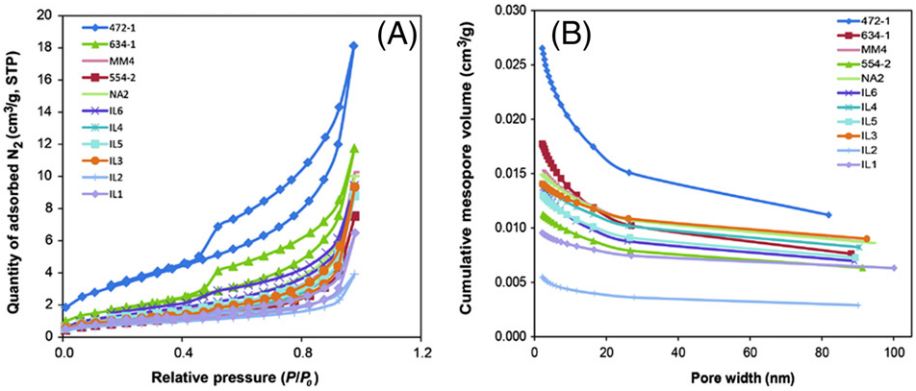

Fig. 4. (A) low-pressure N_2 adsorption isotherms of 60-mesh shale samples. Note that the largest volume of adsorbed N_2 occurs in the least mature sample 472-1, followed by the most organic-rich sample 634-1. (B) Cumulative mesopore volumes of 60-mesh shale samples obtained by low-pressure N_2 adsorption. STP stands for standard temperature and pressure.

no clear relationship with quartz and carbonate abundances (Fig. 8B, C). Similarly, BET surface areas tend to increase with clay contents, and decrease with carbonate and feldspar amounts (except in shale 472-1; Fig. 9). No apparent relationship is observed between average micro- and mesopore sizes and mineralogical compositions (data not shown).

3.3. Comparison of gas adsorption data from 4-, 20-, and 60-mesh shales

Comparative low-pressure gas adsorption porosimetry of particle size fractions yields the following observations:

(1) Mesopore volumes generally increase as particle size decreases, following a trend of $V_{meso\text{-}4}$ $V_{meso\text{-}20}$ $V_{meso\text{-}60}$, except that MM4 and NA2 contain higher $V_{meso\text{-}4}$ than $V_{meso\text{-}20}$ (Fig. 2A, C, Table 3). The evolutionary trends of mesopore volumes with increasing thermal maturity are generally similar for all three shale size fractions (Fig. 2A, C).

(2) Particle size has a stronger relationship with mesopore volume than with micropore volume (Table 3). Twenty- and 60-mesh sizes of shales express similar micropore volumes (Fig. 2B) and thereby differ from 4-mesh fractions with relatively larger micropore volumes in early to intermediately mature samples (R_o 0.55–0.83%).

(3) The TOC content seems to exert stronger control on pore volumes in 20- and 60-mesh samples than in coarser 4-mesh samples. Additionally, the linear regression lines of $V_{meso\text{-}20}$ and $V_{meso\text{-}60}$ versus TOC share similar slopes (Fig. 10).

(4) Hysteresis loops of N_2 adsorption isotherms tighten or even close their openings at low P/P_o from coarsest 4-mesh to finest 60-mesh shale particles (Fig. 11).

4. Discussion

4.1. New Albany Shale pore systems in relation to TOC and mineralogy

The grain size of shale particles used for gas adsorption porosimetry should not strongly affect measurements of meso- and micropore volumes as long as efficient gas transport into and out of the center of each particle allows the entire rock to efficiently reach adsorption equilibrium with gas. With increasing grain size, eventually the core of low-permeability and dense shale fails to reach equilibrium within the time allotted for gas adsorption porosimetry (Clarkson and Bustin, 1999). Consequently, the resulting porosimetric data of larger particle sizes are increasingly biased and reflect mixed signals from an equilibrated periphery and partially equilibrated or non-equilibrated interior rock. The effect of grain size on the measured porosity is clearly demonstrated by the relationships between grain size, porosity, and the abundance of pore-containing OM (Fig. 10). The lack of significant correlations between TOC content (i.e. a proxy for the presence of organic pores) and pore volumes for large 4-mesh particles contrasts against significant correlations for smaller 20-mesh and 60-mesh particle size fractions of the same shales. Moreover, micro- and mesopore volumes of 20-mesh

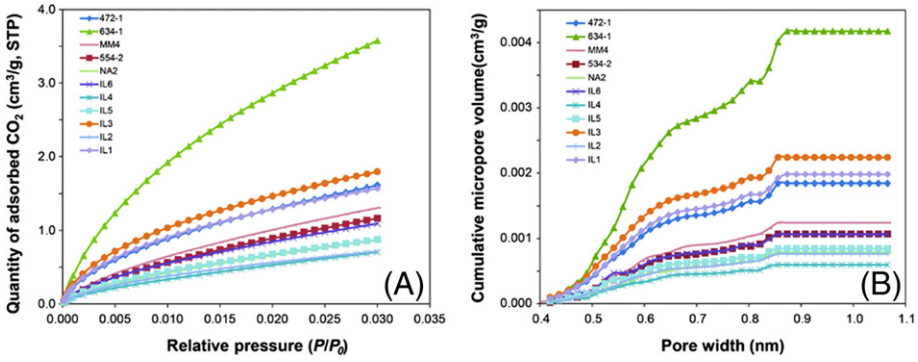

Fig. 5. (A) Low-pressure CO_2 adsorption isotherms of 60-mesh shale samples. Note that the largest volume of adsorbed CO_2 occurs in the most organic-rich sample 634-1. (B) Cumulative micropore volumes of 60-mesh shale samples obtained by low-pressure CO_2 adsorption technique. STP stands for standard temperature and pressure.

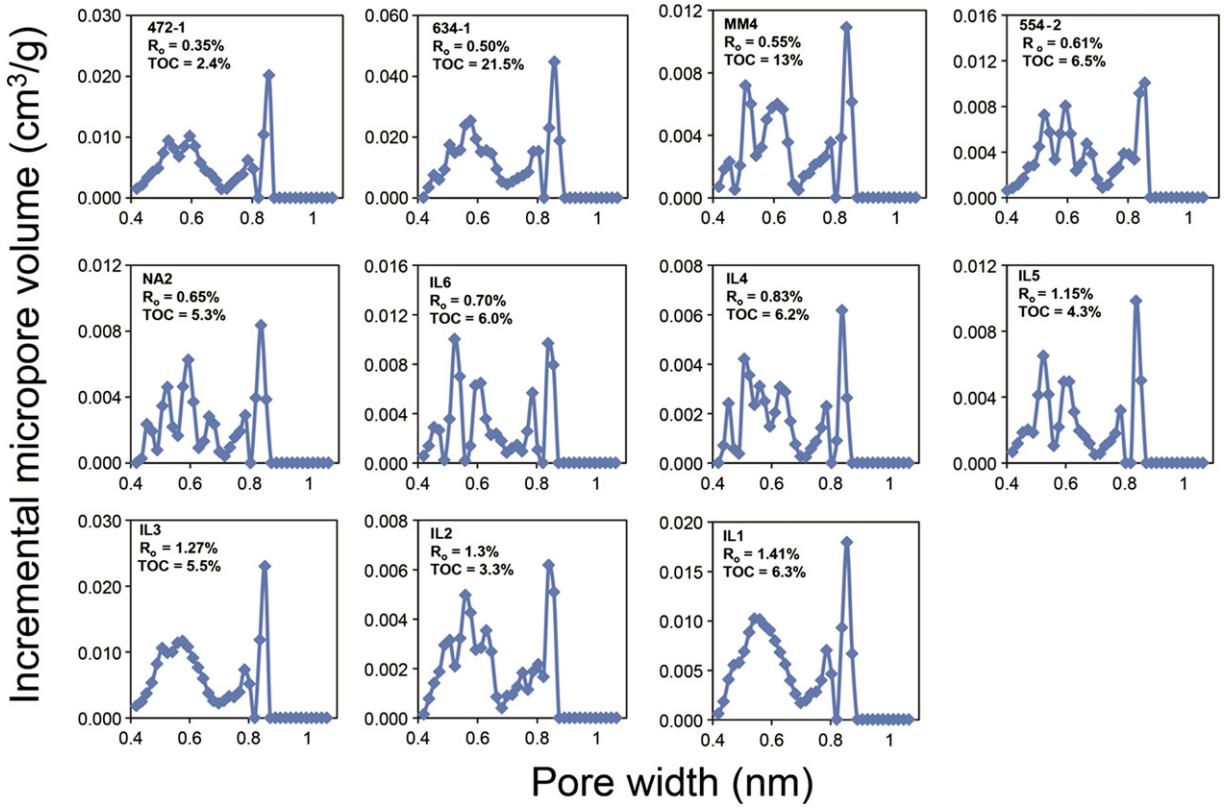

Fig. 6. Incremental micropore volumes of 60-mesh shale samples obtained by low-pressure CO_2 adsorption.

and 60-mesh particles exhibit similar increasing gradients or regression slopes over TOC. It follows that (i) optimized gas adsorption porosimetry uses sufficiently small grain sizes to limit the length of gas flow paths, and (ii) denser, less permeable rocks require smaller grain size samples for valid gas adsorption porosimetry.

We can estimate the contributions of mineral-associated micropores to total micropore volumes by extrapolating the linear regression lines of micropore volume versus TOC to TOC = 0 (Fig. 10), yielding mineralogical micropore volumes of 0.0035 and 0.0052 cm^3/g for 20-mesh and 60-mesh organic-free shales, respectively. OM-associated micropores in the organic-rich shale 634-1 account for more than 70% of the total micropore volume. Similarly, OM-associated mesopore volumes contribute more than half of the total mesopore volume in 634-1.

The influence of TOC content on pore volume is also evident in a comparison of micropore and mesopore volumes in samples IL1 and IL2 that share similar thermal maturity and mineralogical compositions, except that IL1 contains twice as much TOC as IL2 (Table 3). The elevated TOC content in IL1 almost doubles D–A micropore and BJH mesopore volumes compared to IL2. Strong contributions of OM-based pores in gas shales were also reported from the Mississippian Barnett Shale of the Fort Worth Basin, Texas (Loucks et al., 2009, 2012), the Mowry Shale in the Powder River Basin of Wyoming (Modica and Lapierre, 2012), the Chuandong Thrust Fold Belt from southwestern China (Tian et al., 2013), and other shale formations (Jarvie, 1991, Jarvie et al., 2007). The strong influence of TOC on pore volumes underscores the importance of sorption capacity of OM-associated micropores and their collective large pore surface area.

Table 4
Comparison between BET surface areas and average pore sizes derived from N_2 and CO_2 sorption.

	60 mesh		20 mesh		4 mesh	
Sample	N_2-BET	CO_2-BET	N_2-BET	CO_2-BET	N_2-BET	CO_2-BET
472-1	12.2	8.4	11.0	8.3	10.4	8.8
634-1	6.5	21.5	4.6	21.3	1.9	12.9
MM4	4.5	7.9	0.8	7.4	0.2	16.8
554-2	3.3	7.2	0.9	5.5	0.0	21.0
NA2	4.1	5.3	1.2	5.1	0.6	5.9
IL6	5.1	6.2	1.6	5.1	0.3	13.5
IL4	3.7	4.2	0.7	2.6	0.0	1.7
IL5	4.1	5.0	0.7	3.6	0.1	1.9
IL3	3.9	9.4	1.4	8.3	0.5	6.5
IL2	2.7	4.0	2.2	3.4	1.4	3.4
IL1	3.1	8.4	1.6	7.7	0.9	7.4

It is interesting to compare the pore volumes of samples 634-1 and MM4 that share similar R_o values and mineralogical compositions, although 634-1 contains almost twice as much TOC as MM4. The elevated TOC content in 4-mesh 634-1, however, translates only into ~50% of the measured micro- and mesopore volumes in 4-mesh 634-1 (Fig. 2, Table 3). Plausible reasons include (i) problematic porosimetric measurements of 4-mesh samples due to excessive particle size delaying gas adsorption equilibration, (ii) analytical uncertainties rooted in the intrinsic heterogeneity of shale, and (iii) artefacts induced by grain crushing and sieving. These uncertainties will be discussed in Section 4.4.

The ratios of micropore surface area versus TOC from 0.3 to 5.1 cm^3/g in our shales are lower than in Mississippian-Devonian shales in the Western Canadian Sedimentary Basin as reported by Ross and Bustin (2009). In spite of the importance of organic carbon to porosity in shale, obviously there are additional factors such as mineralogy and thermal maturity affecting porosity. Our suite of samples indicates that meso- and micropore volumes as well as surface area tend to increase with higher clay abundance and decrease with enhanced feldspar content (Figs. 8, 9). Clay-associated pores are known to contribute to microporosity in shales (Kuila and Prasad, 2013; Ross and Bustin,

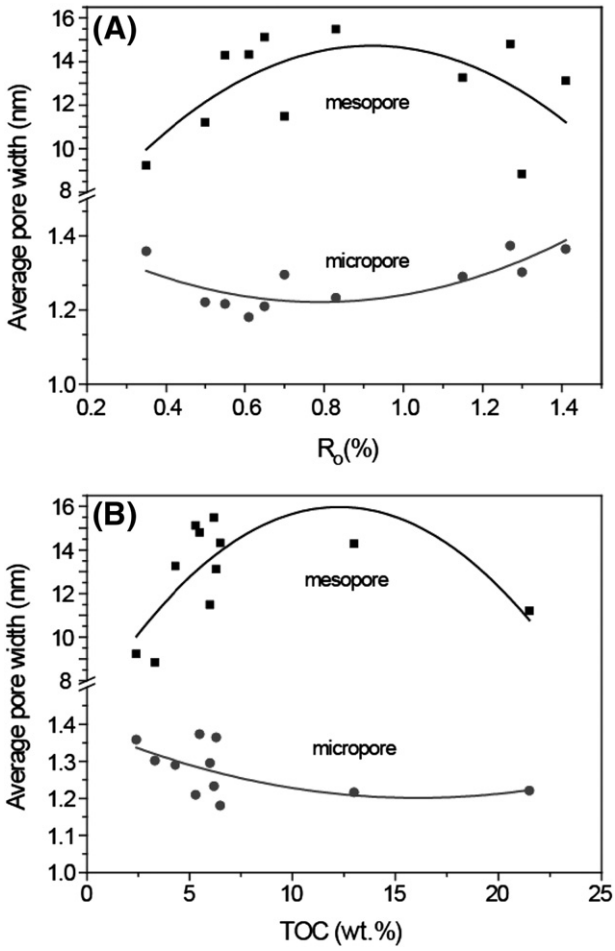

Fig. 7. Relationships between average pore width of mesopores (squares) and micropores (circles) of 60-mesh particles with thermal maturity (A) and TOC content (B). Polynomial regressions were performed to fit the data.

2009; Strąpoć et al., 2010) depending on the degree and type of packing and size of clay crystals (Aylmore and Quirk, 1967).

4.2. Evolution of New Albany Shale pore systems during thermal maturation

The influence of increasing thermal maturation and concurrent geochemical transformation of NAS is reflected by intermittent minima of porosity. An early decrease in mesopore volume from an immature to early mature stage is likely attributed to physical compaction and preferential crushing of mesopores due to increasing pressure of overburden (Mastalerz et al., 2013). The following increase in mesopore volume during the early oil window is associated with the generation of new pores during the thermal degradation of OM ('kerogen cracking'). The oil window's generation of liquid hydrocarbons (bitumen, oil) eventually supplies enough liquids during the late mature stage to cause a decrease in mesopore volume due to the blocking and filling of pore bodies and throats with bitumen, thus restricting the flow of gas and decreasing access to pores. At even higher thermal maturity, ongoing cracking within the gas window generates gaseous hydrocarbons at the expense of oil and bitumen ('secondary cracking'), thereby unblocking bitumen-clogged pores and generating new porosity as non-porous liquid bitumen transforms to solid, porous pyrobitumen (Jarvie et al., 2007; Mastalerz et al., 2013). The generation of new porosity during secondary cracking is witnessed by increased micropore and mesopore volumes in post mature shale IL1 (Fig. 3).

4.3. Effect of particle size on measured pore characteristics

Crushing of shale and the use of smaller particle size fractions in gas adsorption porosimetry result in significantly elevated measured micro- and mesopore volumes, which can be explained by positioning more pores closer to the surface of particles and increasing the portion of pores that are accessible to the gases used in porosimetry. The effect is demonstrated by comparing DFT micropore distributions of grain size fractions of sample IL4 (Fig. 12) where significantly larger micropore volumes and wider micropore size ranges are detected after grinding shales to smaller 20- and 60-mesh sizes.

A close examination of measured micropore volumes along increasing TOC concentrations demonstrates that 20- and 60-mesh samples follow a different evolutionary pattern than coarser 4-mesh samples from the same shales (Fig. 10B). The microporosity in shale should not be significantly affected by manual mild crushing and sieving. The observed difference must therefore be an artefact due to incomplete equilibration of the interior of larger shale particles during gas adsorption porosimetry (Clarkson and Bustin, 1999).

Measurements of micropore volumes via gas adsorption in larger particles may partially include meso- or even macropore volumes. As illustrated in Fig. 13, a large segment of rock contains interconnected pore systems in which large meso- or macropores are connected to multiple micropores. Some of these pore systems may have entrances and interior connecting passages that are too narrow for N_2 but passable for CO_2. Such restrictive situations become more abundant with increasing rock size. Selective access for CO_2 to pore systems that include meso- and even macropores mimics an overly large abundance of micropores. The combined effects of inability to reach adsorption equilibrium and CO_2-selective access to pore networks can weaken the validity of pore volume measurements in large particles.

Based on the results of this study, we suggest that an appropriate rock particle size should be selected for gas adsorption porosimetric measurements. Suarez-Rivera et al. (2012) suggested that crushing of shale to particles of 6 mm diameter effectively removes the influence of coring-induced microcracks on permeability measurements. This conclusion should also apply to porosity measurements of shales. Considering the difficulty to achieve adsorption equilibrium in large 4-mesh samples in a reasonable amount of time (especially for N_2 adsorption at 77 K), we suggest that a particle size below 20 mesh (i.e. 0.85 mm diameter) is preferable for achieving gas adsorption equilibrium and providing a consistent surface area for porosimetry measurements. Excessively small grain size should also be avoided to limit experimental artefacts associated with prolonged crushing. Consistent crushing and sieving should be applied to all samples in order to maintain comparability. Published data from gas adsorption porosimetry should be accompanied by analytical details to facilitate inter-laboratory comparisons of porosity measurements.

4.4. Gas adsorption hysteresis loop

Hysteresis at relative gas pressures from 0.420 to 0.995 indicates capillary condensation at low temperatures within mesopores (Clarkson and Bustin, 1999; Gregg and Sing, 1982; Mastalerz et al., 2013). The lower limit of 0.42 for P/P_o is attributed to the surface tension of liquid N_2 adsorbate reaching an unstable state at a specific pressure (Sing et al., 1985). A close examination of hysteresis loops (e.g., Fig. 11) of our samples reveals that they indicate pores of types H2 and H3 that are usually characterized by narrow necks and wide bodies (referred to as inkbottle-shaped pores), and slit-shaped or spherical pores, respectively (Sing et al., 1985). Caution is advised when adopting this generalizing interpretation for natural shales with structurally more complex pores (Schmitt et al., 2013). Clarkson et al. (2013) reported that the assumption of slit-shape pores inferred from hysteresis loop shapes is not consistent with SANS scattering results. It is now recognized that the role of network effects must be taken into

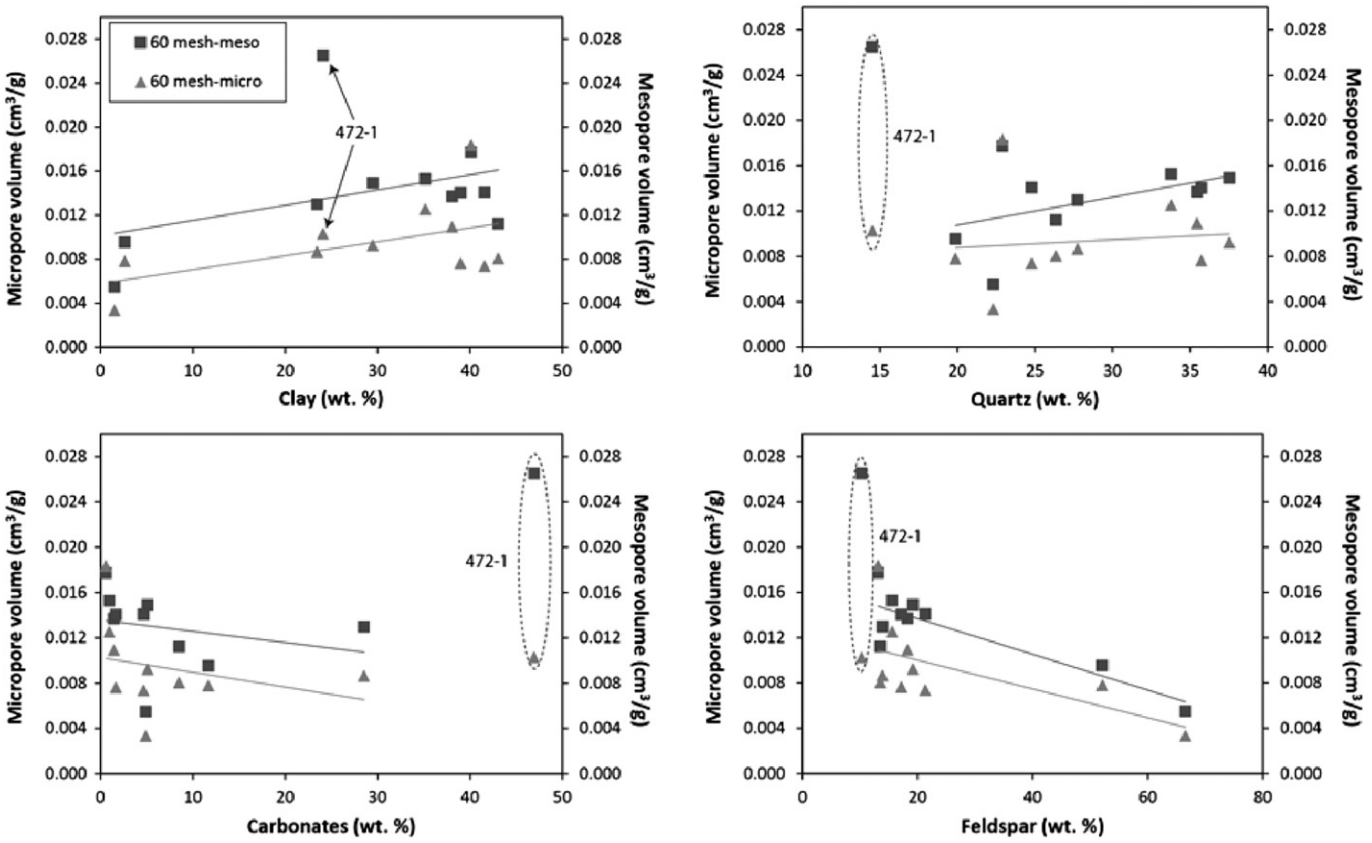

Fig. 8. Relationships between micropore volumes (triangles) and mesopore volumes (squares) in 60-mesh shale samples with distinct mineralogical compositions.

account when interpreting hysteresis loop shapes in terms of pore shapes (Naumov, 2009).

Open hysteresis loops found for many shale samples (Fig. 4) are likely due to trapped gases in narrow pore throats and/or swelling that further constrict pore throats (Gregg and Sing, 1982). Evidence for tighter hysteresis loops associated with smaller particle size (Fig. 11) is possibly related to improved gas transport through pore networks with shorter flow paths and a reduced likelihood of gas being trapped in pore networks during desorption.

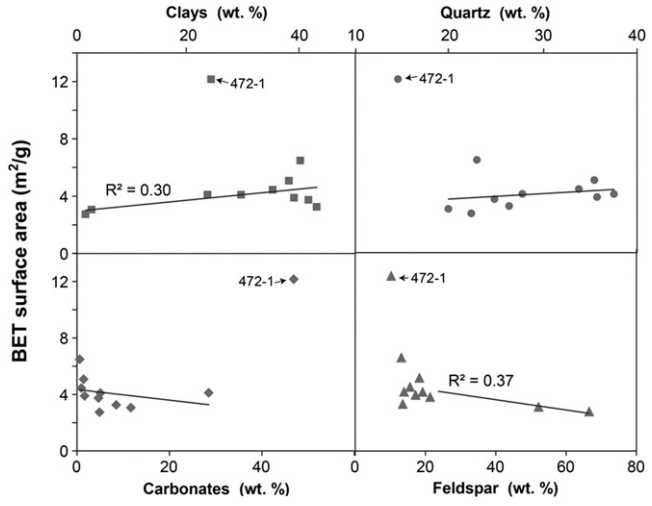

Fig. 9. BET surface areas of 60-mesh shales as a function of distinct mineralogical compositions.

4.5. Uncertainties

The downsizing of particles generally increases measured micro- and mesopore volumes by enhancing pore accessibility. However, this observation is not valid for all samples. Crushing of MM4 and NA2 from 4 mesh to 20 mesh reduced the mesopore volumes (Fig. 2C), and crushing from 4 mesh to 20 or 60 mesh decreased the micropore volumes of MM4, 554-2, NA2, IL6, and IL4 (Fig. 2D). We suspect that the observed deviations are likely associated with less reliable porosimetric data for larger 4-mesh particles, as well as with experimental uncertainties in terms of shale heterogeneity and sample preparation.

The intrinsic heterogeneity of shale in terms of organic and mineral composition, texture, fabric, etc., makes it fundamentally impossible to prepare petrologically and chemically identical size fractions. Nonetheless, the impact of this bias should be limited because (i) bulk shale samples were crushed into chips and well homogenized before division into three aliquots and final crushing into three size fractions, (ii) a relatively large ~2-g amount of sample was used for each measurement, (iii) multiple sub-sampling and crushing of bulk shale allowed independent repeat experiments of size fractions with comparable porosimetric results.

Crushing uses compression and shear forces to induce fracture propagation and generate smaller fragments (Mowar et al., 1996). Changes in structure and fabric at the microscopic level inevitably alter surface properties and may entail pore collapse or the generation of new porosity (Lee, 2012; Liu et al., 2012) along with experimental errors in porosimetry (Boudriche et al., 2014; Lee, 2012). Our slow manual grinding of shales for less than 20 min in an agate mortar should have limited such artefacts because the associated mechanical forces are unlikely to provide the critical stress needed for pore collapse (40 MPa for Cordoba Cream limestone, Texas, US; Mowar et al., 1996) and significant pore volume change.

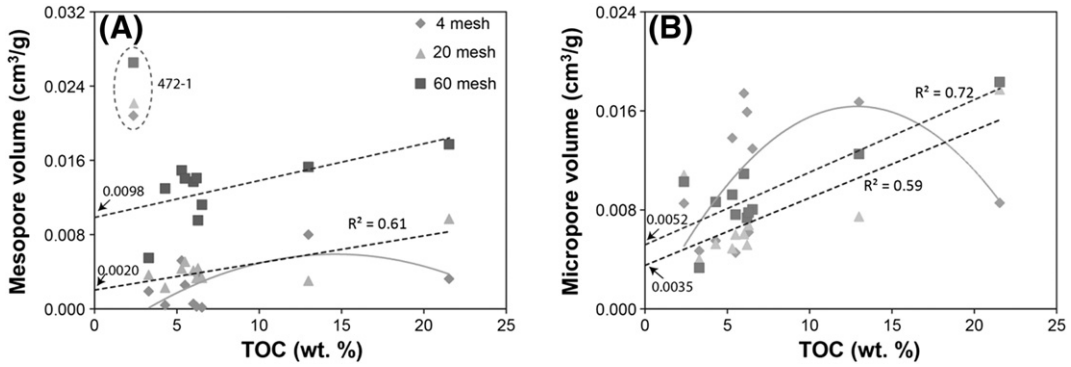

Fig. 10. Relationships of mesopore volumes (A) and micropore volumes (B) of varying particle sizes with TOC contents. Linear regressions were performed for 20- and 60-mesh particle sizes, and trend lines of 4-mesh shales were drawn to guide the eye.

5. Conclusions

Pore structure analyses have been applied to a suite of 11 New Albany Shale samples with different thermal maturities to constrain fundamental controls on gas adsorption capacities in fine-grained shales, and by extension to mudstones. The following main conclusions have been reached:

1. Primary cracking of kerogen and secondary cracking of bitumen along increasing thermal maturity cause mesopore volumes to follow a nonlinear path with multiple intermittent minima. In contrast, micropore volumes seem to be controlled dominantly by the abundance of organic matter. Clay and feldspar contents exert additional effects on microporosity, mesoporosity, and surface areas.
2. The rock particle size used for gas adsorption porosimetry strongly influences porosimetric results. Measured pore volumes generally increase with decreasing particle size, especially with particle sizes 20 mesh. Gas adsorption hysteresis loops tend to be tightened or remain close with decreasing particle size at low P/P_o because shorter gas transport paths facilitate access to pores and diminish the possibility of gas remaining trapped during desorption.

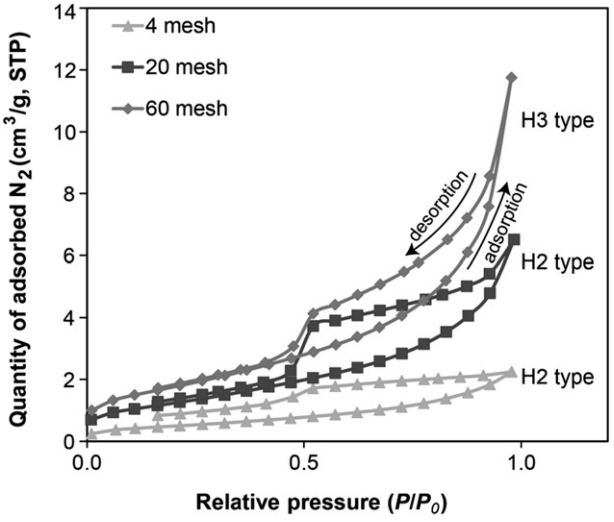

Fig. 11. N_2 adsorption isotherms of different size fractions of shale sample 634-1. Note that the openings of hysteresis patterns get tighter from coarsest 4-mesh to finest 60-mesh shale particle sizes. The hysteresis pattern shifts from type H2 in 4-mesh and 20-mesh samples (i.e. inkbottle-shaped and polymorphic pores hindering gas transport) to type H3 for 60-mesh samples (i.e. slit-shaped or spherical pores). STP stands for standard temperature and pressure. The arrows indicate the directions of pressure change during adsorption and desorption.

Complex pore structures and pore size distributions in shales complicate experimental porosimetric characterizations. Reliable predictions of adsorbed gas capacities of shales cannot be based on single attributes but need to be based jointly on the organic matter (or total organic carbon) content, mineralogy, and thermal maturity. It is imperative to select a suitably small particle size for rock fragments in gas adsorption porosimetry to limit analytical bias due to incomplete equilibration of larger particles. Future research on porosity in shales will require a multidisciplinary approach to evaluate the influence of additional reservoir parameters, for example kerogen type, the possible presence of migrated hydrocarbons, lithostatic pressure (grain-supported) by overburden, reservoir temperature, the presence of formation water, the salinity of formation water, and mineral diagenesis.

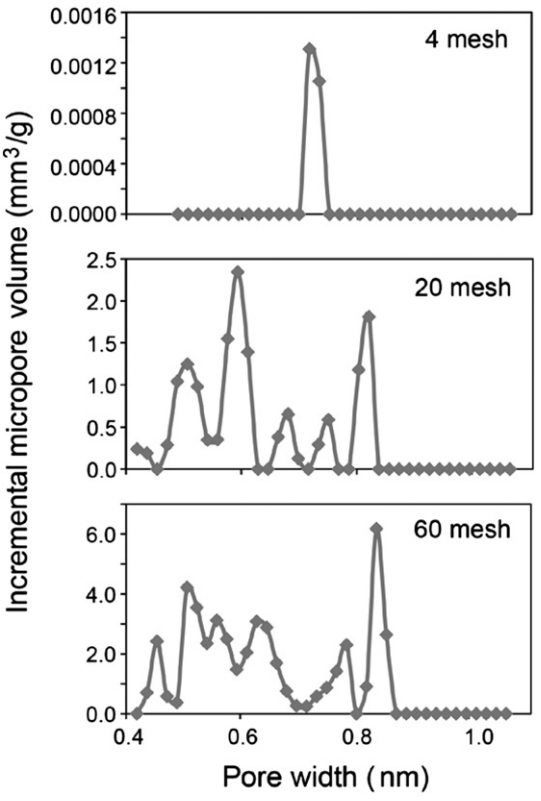

Fig. 12. Comparison of micropore volume distributions in varying size fractions of sample IL4.

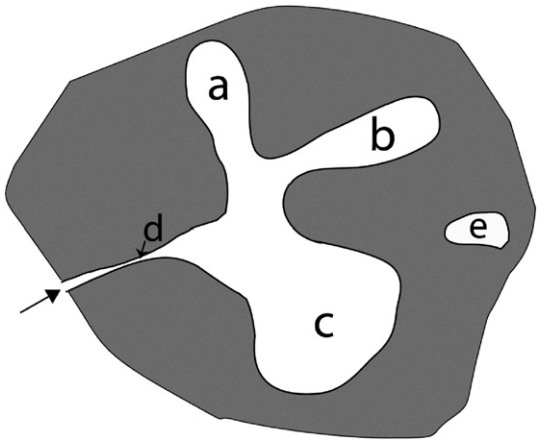

Fig. 13. Adsorption measurements are influenced by porosity networks featuring interconnected mesopores (a, b), macropores (c), and micropores (d). Pore (e) is a closed pore.

Acknowledgments

Financial support from the China Scholarship Council (CSC) for Y. C. and L. W. is gratefully acknowledged. Y. C. also thanks the college of Art and Science at Indiana University for the 1-year dissertation fellowship. This material is based upon work supported by the U.S. Department of Energy, Office of Science, Office of Basic Energy Sciences under Award Number DE-SC0006978 (formerly DE-FG02-11ER16246). The manuscript greatly benefited from constructive comments of two reviewers.

References

Aylmore, L.A.G., Quirk, J.P., 1967. The micropore size distributions of clay mineral systems. J. Soil Sci. 18, 1–17.

Bernard, S., Horsfield, B., Schulz, H.-M., Wirth, R., Schreiber, A., Sherwood, N., 2012. Geochemical evolution of organic-rich shales with increasing maturity: a STXM and TEM study of the Posidonia Shale (Lower Toarcian, northern Germany). Mar. Pet. Geol. 31, 70–89.

Borchardt, L., Oschatz, M., Paasch, S., Kaskel, S., Brunner, E., 2013. Interaction of electrolyte molecules with carbon materials of well-defined porosity: characterization by solid-state NMR spectroscopy. Phys. Chem. Chem. Phys. 15, 15177–15184.

Boudriche, L., Chamayou, A., Calvet, R., Hamdi, B., Balard, H., 2014. Influence of different dry milling processes on the properties of an attapulgite clay, contribution of inverse gas chromatography. Powder Technol. 254, 352–363.

Chalmers, G.R.L., Bustin, R.M., 2012. Light volatile liquid and gas shale reservoir potential of the Cretaceous Shaftebury Formation in northeastern British Columbia. Canada. AAPG Bulletin 96, 1333–1367.

Chalmers, G.R., Bustin, R.M., Power, I.M., 2012. Characterization of gas shale pore systems by porosimetry, pycnometry, surface area, and field emission scanning electron microscopy/transmission electron microscopy image analyses: examples from the Barnett, Woodford, Haynesville, Marcellus, and Doig units. AAPG Bull. 96, 1099–1119.

Clarkson, C.R., Bustin, R.M., 1999. The effect of pore structure and gas pressure upon the transport properties of coal: a laboratory and modeling study. 1. Isotherms and pore volume distributions. Fuel 78, 1333–1344.

Clarkson, C.R., Freeman, M., He, L., Agamalian, M., Melnichenko, Y.B., Mastalerz, M., Bustin, R.M., Radliński, A.P., Blach, T.P., 2012. Characterization of tight gas reservoir pore structure using USANS/SANS and gas adsorption analysis. Fuel 95, 371–385.

Clarkson, C.R., Solano, N., Bustin, R.M., Bustin, A.M.M., Chalmers, G.R.L., He, L., Melnichenko, Y.B., Radliński, A.P., Blach, T.P., 2013. Pore structure characterization of North American shale gas reservoirs using USANS/SANS, gas adsorption, and mercury intrusion. Fuel 103, 606–616.

Cui, X., Bustin, A.M.M., Bustin, R.M., 2009. Measurements of gas permeability and diffusivity of tight reservoir rocks: different approaches and their applications. Geofluids 9, 208–223.

Curtis, M.E., Cardott, B.J., Sondergeld, C.H., Rai, C.S., 2012. Development of organic porosity in the Woodford Shale with increasing thermal maturity. Int. J. Coal Geol. 103, 26–31.

Gregg, S.J., Sing, K.S.W., 1982. Adsorption, Surface Area and Porosity. second edition. Academic Press, New York.

Jarvie, D.M., 1991. Total organic carbon (TOC) analysis. In: Merrill, R.K. (Ed.), Source and Migration Processes and Evaluation Techniques: AAPG Treatise of Petroleum Geology, Handbook of Petroleum Geology. American Association of Petroleum Geologist, Tulsa, pp. 113–118.

Jarvie, D.M., Hill, R.J., Ruble, T.E., Pollastro, R.M., 2007. Unconventional shale-gas systems: the Mississippian Barnett Shale of north-central Texas as one model for thermogenic shale-gas assessment. AAPG Bull. 91, 475–499.

Kuila, U., Prasad, M., 2013. Specific surface area and pore-size distribution in clays and shales. Geophys. Prospect. 61, 341–362.

Lee, J., 2012. Grinding effects on the change of particle properties in cupric sulfide, CuS. Adv. Powder Technol. 23, 731–735.

Liu, Y., Wang, W., Wang, A., 2012. Effects of dry grinding on the microstructure of palygorskite and adsorption efficiency for methylene blue. Powder Technol. 225, 124–129.

Loucks, R.G., Reed, R.M., Ruppel, S.C., Jarvie, D.M., 2009. Morphology, genesis, and distribution of nanometer-scale pores in siliceous mudstones of the Mississippian Barnett Shale. J. Sediment. Res. 79, 848–861.

Loucks, R.G., Reed, R.M., Ruppel, S.C., Hammes, U., 2012. Spectrum of pore types and networks in mudrocks and a descriptive classification for matrix-related mudrock pores. AAPG Bull. 96, 1071–1098.

Lowell, S., Shields, J.E., Thomas, M.A., Thommes, M., 2004. Characterization of Porous Solids and Powders: Surface Areas, Pore Size and Density. Kluwer Academic Publishers, The Netherlands.

Mastalerz, M., He, L., Melnichenko, Y.B., Rupp, J.A., 2012. Porosity of coal and shale: insights from gas adsorption and SANS/USANS techniques. Energy Fuel 26, 5109–5120.

Mastalerz, M., Schimmelmann, A., Drobniak, A., Chen, Y., 2013. Porosity of Devonian and Mississippian New Albany Shale across a maturation gradient: insights from organic petrology, gas adsorption, and mercury intrusion. AAPG Bull. 97, 1621–1643.

Modica, C.J., Lapierre, S.G., 2012. Estimation of kerogen porosity in source rocks as a function of thermal transformation: example from the Mowry Shale in the Powder River Basin of Wyoming. AAPG Bull. 96, 87–108.

Mowar, S., Zaman, M., Stearns, D.W., Roegiers, J.C., 1996. Micro-mechanisms of pore collapse in limestone. J. Pet. Sci. Eng. 15, 221–235.

Naumov, S., 2009. Hysteresis phenomena in mesoporous materials. (Doctoral dissertation), Universität Leipzig (105 pp.).

Peters, K.E., Cassa, M.R., 1994. Applied source rock geochemistry. In: Magoon, L.B., Dow, W.G. (Eds.), The Petroleum System—from Source to Trap. American Association of Petroleum Geologists Memoir 60. American Association of Petroleum Geologist, Tulsa, pp. 93–120.

Ross, D.J.K., Bustin, R.M., 2007. Shale gas potential of the Lower Jurassic Gordondale Member, northeastern British Columbia, Canada. Bull. Can. Petrol. Geol. 55, 51–75.

Ross, D.J.K., Bustin, R.M., 2009. The importance of shale composition and pore structure upon gas storage potential of shale gas reservoirs. Mar. Pet. Geol. 26, 916–927.

Schieber, J., 2010. Common themes in the formation and preservation of intrinsic porosity in shales and mudstones — illustrated with examples across the Phanerozoic. Society of Petroleum Engineers Unconventional Gas Conference, Pittsburgh, Pennsylvania, February 23–25, 2010. SPE Paper 132370 (12 pp.).

Schieber, J., 2011. Shale microfabrics and pore development — an overview with emphasis on the importance of depositional processes. In: Leckie, D.A., Barclay, J.E. (Eds.), Gas Shale of the Horn River Basin. Canadian Society of Petroleum Geologists, Calgary, pp. 115–119.

Schmitt, M., Fernandes, C.P., da Cunha Neto, J.A.B., Wolf, F.G., dos Santos, V.S.S., 2013. Characterization of pore systems in seal rocks using nitrogen gas adsorption combined with mercury injection capillary pressure techniques. Mar. Pet. Geol. 39, 138–149.

Sing, K.S.W., Everett, D.H., Haul, R.A.W., Moscou, L., Pierotti, R.A., Rouquérol, J., Siemieniewska, T., 1985. Reporting physisorption data for gas/solid systems with special reference to the determination of surface area and porosity. Pure Appl. Chem. 57, 603–619.

Strąpoć, D., Mastalerz, M., Schimmelmann, A., Drobniak, A., Hasenmueller, N.R., 2010. Geochemical constraints on the origin and volume of gas in the New Albany Shale (Devonian–Mississippian), eastern Illinois Basin. AAPG Bull. 94, 1713–1740.

Suarez-Rivera, R., Chertov, M., Willberg, D., Green, S., Keller, J., 2012. Understanding permeability measurements in tight shales promotes enhanced determination of reservoir quality. Paper prepared for presentation at the SPE Canadian Unconventional Resources Conference held in Calgary, Alberta, Canada, 30 October–1 November 2012. Soc. Petrol. Eng., SPE 162816, pp. 1–13.

Tian, H., Pan, L., Xiao, X., Wilkins, R.W.T., Meng, Z., Huang, B., 2013. A preliminary study on the pore characterization of Lower Silurian black shales in the Chuandong Thrust Fold Belt, southwestern China using low pressure N_2 adsorption and FE-SEM methods. Mar. Pet. Geol. 48, 8–19.

Walters, C.C., 2013. New insights on gas storage and transport in shales. Goldschmidt 2013 Conference, Abstracts, p. 2443 (http://goldschmidt.info/2013/abstracts/finalPDFs/2443.pdf).